European Journal of Cell Biology 102 (2023) 151285

Contents lists available at ScienceDirect

European Journal of Cell Biology

journal homepage: www.elsevier.com/locate/ejcb

Phospholipid fatty acid remodeling and carbonylated protein increase in extracellular vesicles released by airway epithelial cells exposed to cigarette smoke extract

Elisabetta Chiaradia [a,1], Anna Sansone [b,1], Carla Ferreri [b], Brunella Tancini [c], Raffaella Latella [c], Alessia Tognoloni [a], Angela Gambelunghe [d], Marco dell'Omo [d], Lorena Urbanelli [c], Stefano Giovagnoli [e], Roberto Maria Pellegrino [c], Giada Cerrotti [c], Carla Emiliani [c,*], Sandra Buratta [c,*]

[a] Department of Veterinary Medicine, University of Perugia, Perugia, Italy
[b] ISOF, Consiglio Nazionale delle Ricerche, Bologna, Italy
[c] Department of Chemistry, Biology and Biotechnology, University of Perugia, Perugia, Italy
[d] Department of Medicine, University of Perugia, Perugia, Italy
[e] Department of Pharmaceutical Sciences, University of Perugia, Perugia, Italy

ARTICLE INFO

Keywords:
Extracellular Vesicles
Airway epithelial cells
Cigarette smoke extract
Protein carbonylation
Phospholipid fatty acids
Trans fatty acid isomers

ABSTRACT

Cigarette smoke (CS) represents one of the most relevant environmental risk factors for several chronic pathologies. Tissue damage caused by CS exposure is mediated, at least in part, by oxidative stress induced by its toxic and pro-oxidant components. Evidence demonstrates that extracellular vesicles (EVs) released by various cell types exposed to CS extract (CSE) are characterized by altered biochemical cargo and gained pathological properties. In the present study, we evaluated the content of oxidized proteins and phospholipid fatty acid profiles of EVs released by human bronchial epithelial BEAS-2B cells treated with CSE. This specific molecular characterization has hitherto not been performed. After confirmation that CSE reduces viability of BEAS-2B cells and elevates intracellular ROS levels, in a dose-dependent manner, we demonstrated that 24 h exposure at 1% CSE, a concentration that only slight modifies cell viability but increases ROS levels, was able to increase carbonylated protein levels in cells and released EVs. The release of oxidatively modified proteins *via* EVs might represent a mechanism used by cells to remove toxic proteins in order to avoid their intracellular overloading. Moreover, 1% CSE induced only few changes in the fatty acid asset in BEAS-2B cell membrane phospholipids, whereas several rearrangements were observed in EVs released by CSE-treated cells. The impact of changes in acyl chain composition of CSE-EVs accounted for the increased saturation levels of phospholipids, a membrane parameter that might influence EV stability, uptake and, at least in part, EV-mediated biological effects. The present *in vitro* study adds new information concerning the biochemical composition of CSE-related EVs, useful to predict their biological effects on target cells. Furthermore, the information regarding the presence of oxidized proteins and the specific membrane features of CSE-related EVs can be useful to define the utilization of circulating EVs as marker for diagnosing of CS-induced lung damage and/or CS-related diseases.

1. Introduction

Extracellular vesicles (EVs) are a heterogeneous group of membrane-surrounded particles secreted by almost all cell types in response to a variety of physiological and exogenous stimuli. EVs are commonly classified on the basis of their origin, size and expression markers. Based

* Corresponding authors.
E-mail addresses: elisabetta.chiaradia@unipg.it (E. Chiaradia), anna.sansone@isof.cnr.it.it (A. Sansone), carla.ferreri@isof.cnr.it (C. Ferreri), brunella.tancini@unipg.it (B. Tancini), raffaella.latella@studenti.unipg.it (R. Latella), alessia.tognoloni@studenti.unipg.it (A. Tognoloni), angela.gambelunghe@unipg.it (A. Gambelunghe), marco.dellomo@unipg.it (M. dell'Omo), lorena.urbanelli@unipg.it (L. Urbanelli), stefano.giovagnoli@unipg.it (S. Giovagnoli), roberto.pellegrino@unipg.it (R.M. Pellegrino), giada.cerrotti@studenti.unipg.it (G. Cerrotti), carla.emiliani@unipg.it (C. Emiliani), sandra.buratta@unipg.it (S. Buratta).
[1] These authors contributed equally to this work.

https://doi.org/10.1016/j.ejcb.2022.151285
Received 16 June 2022; Received in revised form 14 December 2022; Accepted 17 December 2022
Available online 26 December 2022
0171-9335/© 2022 The Author(s). Published by Elsevier GmbH. This is an open access article under the CC BY-NC-ND license (http://creativecommons.org/licenses/by-nc-nd/4.0/).

on their origin, EVs have been defined as microvesicles (<100 or 200 nm), which directly bud from the plasma membrane, apoptotic blebs (>1000 nm), which are released by cells undergoing apoptosis, and exosomes (50–150 nm), which are secreted *via* exocytosis from late endosome multivesicular bodies (MVBs) (Urbanelli et al., 2013; Théry et al., 2018). However, exosome and microvesicles share partially overlapping biophysical (*i.e.* size and density) and biochemical (*i.e.* surface markers) characteristics and EVs isolated by size-based methods are heterogenous as it is not possible to separate vesicle subtypes (Théry et al., 2018).

EV content is characterized by the presence of biochemically relevant molecules such as nucleic acids, proteins and lipids which reflect the physio-pathological status of the parental cell (Abels et al., 2016; Llorente et al., 2013; Sagini et al., 2018a). Besides their role in eliminating unnecessary or toxic material, EVs are involved in many biological processes by delivering their molecular cargo to neighboring and distant cells in both physiological and pathological conditions (Robbins et al., 2016; Yokoi et al., 2017; Chiaradia et al., 2021; Tancini et al., 2019). In particular, it has been reported that EVs participate to cellular communication, immune response and inflammation processes (Harischandra et al., 2017; Sagini et al., 2018b; Haque et al., 2020). Consequently, EVs have gained increasing interest as a source of circulating biomarkers useful for diagnostic, prognostic and therapeutic applications in many diseases.

Cigarette smoke (CS) represents one of the most relevant environmental risk factors for several chronic pathologies including cardiovascular diseases, oral and lung cancer and chronic obstructive pulmonary disease (COPD) (Ryu et al., 2018). Most tissue damage caused by CS exposure is mediated by a large number of toxic and pro-oxidant molecules, which are able to induce oxidative stress damage by promoting protein oxidation, DNA damage and lipid peroxidation with detrimental consequences for cell integrity and function (Colombo et al., 2019).

Redox proteomic studies revealed that exposure of epithelial bronchial cells to CSE induces carbonylation of a large number of proteins involved in fundamental metabolic and cellular processes, thus confirming that the reactive species contained in the CSE greatly influence homeostasis and cellular functions (Colombo et al., 2019). Reactive oxidizing molecules could also promote lipid peroxidation, in particular of polyunsaturated fatty acids (PUFA). Garbin et al. (2009) demonstrated that CS induces an alteration of lipid profile in peripheral blood mononuclear cells of young heavy smokers by formation of oxidized phospholipids, which is associated with the activation of Nrf2/ARE pathway.

Recently, numerous studies have also demonstrated that cell exposure to CS increases EV release. High levels of circulating EVs have been found in biological fluids of smokers (Gordon et al., 2011; Mobarrez et al., 2014). In vitro studies showed that exposure to cigarette smoke extract (CSE) induces EV release by different cell types, including airway epithelial cells (Saxena et al., 2021; Benedikter et al., 2017). The CSE-induced release of EVs seems to be related, at least in part, to oxidative stress insult induced by CSE in originating cells. Consistently, it has been demonstrated that oxidative stress affects the release and the molecular content of EVs which, consequently, can deliver their cargo to neighboring cells altering their metabolism and spreading oxidative damage (Chiaradia et al., 2021; Yarana, 2018). Benedikter et al. (2017) demonstrated that reactive compounds like acrolein, contained within CS, contribute to the release of exosomes by airway epithelial cells by depleting cell surface thiol groups and this effect can be prevented by the thiol-based antioxidant systems, such as N-acetyl cysteine and glutathione S-transferase.

It has been reported that EVs secreted under CS exposure show pathological properties and can induce cellular responses that can contribute to CS-related chronic diseases (Ryu et al., 2018; Fujita et al., 2015; Benedikter et al., 2018). For instance, EVs derived from bronchial epithelial cells exposed to CSE may have a crucial pathogenic role in the development of lung cancer and COPD (Fujita et al., 2015). CS-related EVs have been found to induce endothelial dysfunction, tissue remodeling and angiogenesis (Benedikter et al., 2018; Ryu et al., 2018). In addition, pro-inflammatory and pro-coagulant properties of EVs secreted by monocytes and macrophages, as well as by airway epithelial cells exposed to CS have been reported (Haque et al., 2020; Li et al., 2010; Benedikter et al., 2019).

Despite that the correlation between CS-induced damage and the crucial role played by CS-induced EVs in the pathogenesis of smoke-related diseases has been clearly evidenced, studies analyzing the molecular composition of EVs released by CSE-treated airway epithelial cells are very scarce. In particular, results have been reported concerning the analysis of changes in the protein and RNA profiles of EVs from airway epithelial cells (Benedikter et al., 2019; Corsello et al., 2019). Here, we evaluated the presence of carbonylated proteins and changes in lipid profiles of EVs released by human bronchial epithelial BEAS-2B cells treated with CSE, a cell model representative of how cells lining the bronchial tree may function *in vivo*. Detailed characterization of the biochemical cargo of EVs released by CSE-treated cells can shed light on the molecular mechanism underlying CSE effects on target cells. Knowledge derived from our *in vitro* study adds new information regarding the molecular cargo of CSE-related EVs, useful to define the potential use of circulating EVs as diagnostic tool for CS-associated diseases.

2. Materials and methods

2.1. Materials

All culture reagents were from Euroclone S.p.A (Pero, Italy). *Cis* and *trans* fatty acid methyl esters (FAME), dimethyl disulfide, iodine, cholesterol, sphingomyelin, sodium thiosulphate and Iodine were purchased from Merck Life Science (Darmstadt, Germany) and used without further purification; sapienic acid methyl ester, 8cis-18:1 methyl ester and sebaleic acid methyl ester were purchased from Lipidox (Lidingö, Sweden). The solvents chloroform, methanol, isopropanol, diethyl ether and *n*-hexane (HPLC grade) were purchased from Millinckrodt (Phillipsburg, NJ, USA) and used without further purification. POPC (1-palmitoyl-2-oleoyl-sn-glycero-3-phosphocholine), POPE (1-palmitoyl-2-oleoyl-sn-glycero-3-phosphoethanolamine) and POPS (1-palmitoyl-2-oleoyl-sn-glycero-3-phosphoserine) were purchased from Larodan (Solna, Sweden) and used without further purification. Silica gel analytical thin-layer chromatography (TLC) was performed on Merck silica gel 60 plates of 0.25 mm thickness (Merck Life Science) and spots were detected by spraying the plate with a cerium ammonium sulfate/ammonium molybdate reagent. qEVoriginal/70 nm columns were purchased from Schaefer South-East Europe Srl (Rovigo, Italy). All other reagents were from Merck Life Science.

2.2. Cigarette smoke extract (CSE)

CSE was prepared according to previous studies (Benedikter et al., 2019; Zhang et al., 2018), with some modifications. After the removal of the filter, the smoke of one cigarette (Marlboro, Philip Morris, Inc., Richmond, VA, containing 10 mg of tar and 0.8 mg of nicotine) was bubbled through 10 mL of cell culture medium with the use of an experimenter-operated syringe (50 mL). After lighting the cigarette, the mainstream smoke was drawn on the syringe up to 50 mL. The puff should be slow and last 2–4 s. Puffs were repeated every 30 s until the marking on the cigarette was reached. The CSE solution was filtered through a 0.45 μm pore-sized filter to remove bacteria and particulate. This solution was considered to be 100% CSE. To ensure the standardization between experiments, the absorbance of the CSE solution at 320 nm was measured. CSE solution was used when the optical density of 100% CSE was 0.9–0.95 (Saxena et al., 2021). For each experiment, CSE was freshly prepared before use and diluted to an appropriate

concentration with cell culture medium.

2.3. Cell culture and treatments

Human bronchial epithelial BEAS-2B cells were grown in Dulbecco's modified Eagle's medium (DMEM) supplemented with 10% (v/v) heat-inactivated fetal bovine serum (FBS), 100 U/mL penicillin and 100 U/mL streptomycin. Cells were maintained in a humidified 5% CO_2 atmosphere at 37 °C and passaged as needed. For experiments, BEAS-2B cells were seeded in complete medium and allowed to attach for 24 h. Then, the culture medium was carefully removed and cells were washed twice with phosphate-buffered saline (PBS). BEAS-2B cells were incubated for 24 h in the absence (controls) or in presence of various concentration of CSE. To avoid any contamination by lipidic/proteic complexes and lipoproteins present in FBS, all experiments were carried out in serum free medium. In particular: 1×10^4 cells were seeded onto 96-well plates for MTT assay and onto 96-well black plates to determine intracellular ROS concentration; 1.5×10^6 cells were seeded onto cell culture flasks (25 cm^2) to evaluate carbonylated proteins; 4×10^6 were seeded onto cell culture flasks (75 cm^2) for EV isolation from culture media.

2.4. Evaluation of cell viability

Following exposure to CSE, media were removed and cells were treated for 3 h with thiazolyl blue tetrazolium bromide (MTT; 2 mg/mL). Then, dark blue formazan crystals were solubilized in DMSO and the absorbance of dissolved formazan was measured at 570 nm using a microplate reader (Beckman Coulter DTX880). The percentage of viable cells was calculated using the following formula: (absorbance of CSE-treated wells/absorbance of control wells) x 100.

2.5. Evaluation of intracellular ROS production

Intracellular ROS levels were measured using the H_2DCFHDA method (LeBel et al., 1992), with some modifications. Following exposure to different CSE concentrations, cells were washed with PBS and incubated for 60 min with 20 μM H_2DCFDA at 37 °C. Then, cells were washed three times with PBS and the fluorescence intensity of the oxidized form of DCF was measured at excitation/emission wavelengths of 485/530 nm using a microplate reader (DTX880 Multimode Detector, Beckman Coulter). Data, expressed as percentage of DCF fluorescence with respect to control, were normalized to cell viability evaluated by MTT assay.

2.6. Evaluation of lipid peroxidation

Lipid peroxidation was assessed by measuring the production of thiobarbituric acid-reactive substances (TBARS) of malondialdehyde (MDA), according to the method proposed by Draper and Hadley (1990). Cell lysate supernatants were mixed with TBA solution (0.1% thiobarbituric acid, 10%TCA and 0.01% BHT) and heated for 45 min at 95 °C. After cooling in ice, 0.5 mL of n-butanol were added, mixed and finally centrifugated at 200xg for 10 min. The butanol phase was then transferred to 96-well plate and absorbance was measured at 532 nm using microplate reader Tecan infinitive (TECAN, USA). MDA concentrations were calculated using 1,1,3,3-tetramethoxypropane standard curve and normalized to total protein concentration.

2.7. EV isolation

BEAS-2B cells were incubated for 24 h in the absence (controls) (three flasks) or in the presence of 1% CSE (three flasks), as described above. Then, media were collected to isolate EVs by differential centrifugation protocol (Kowal et al., 2016; Buratta et al., 2021). Briefly, media were subjected to low-speed centrifugations to remove cells, cell debris and large EVs (300xg for 10 min; 2,000xg for 10 min; 10,000xg for 30 min). Supernatants were then ultracentrifuged at 100,000xg for 70 min to pellet EVs, which were washed in PBS and centrifuged again at 100,000xg for 70 min. The final pellets were re-suspended in small volume (100–150 μl) of filtered (0.22 μm pore size) PBS and used for further analyses. In some cases, EVs recovered by the last step of ultracentrifugation were further purified using Size Exclusion Chromatography (SEC). In particular, EVs (40 μg) were loaded on the top of an qEV/70 nm SEC column (Izon Science) and eluted with PBS, following manufacturer's instructions. Twenty fractions of 0,5 mL were collected. The EV-containing fractions were identified by western blotting using an antibody against the EV protein marker CD81.

2.8. EV Characterization

2.8.1. Scanning electron microscopy, nanoparticle tracking analysis and cryo-transmission electron microscopy

Scanning Electron Microscopy (SEM) examination was carried out according to previous studies (Buratta et al., 2017, 2021). EVs were fixed in 2.5% glutaraldehyde for 15 min at room temperature, washed twice with large volume of water using Vivaspin concentration devices (300,000 Da cut-off), then sedimented on glass coverslips and allowed to dry at room temperature. SEM images were obtained using a field emission LEO 1525 electron scanning microscope (Zeiss, Thornwood, USA) equipped with a Gemini column, after Cr metallization using a high-resolution sputter Q150T ES-Quorum apparatus (24 s sputter at a current of 20 mA). Chromium thickness was ~10 nm.

A Malvern Panalytical NanoSight NS300 Nanoparticle Tracking Analysis (NTA) system (Malvern, Worcestershire, UK) was used to assess the EV concentration and size distribution. EVs were resuspended and diluted in filtered PBS to be suitable for the NTA system's working concentration range and five measurements were performed for each one. The analysis of EVs from two independent experiments has been carried out.

Samples for cryo-Transmission Electron Microscopy (cryo-TEM) analysis were prepared by placing a drop of 5 μl EV samples on a Quantifoil Multi A holey carbon-coated copper grid (copper R2/1, Quantifoil Micro Tools GmbH) that were previously glow discharged. Excess fluid was blotted from the grid and plunge frozen in liquid ethane using a FEI Vitrobot Mark IV plunge freezer to achieve sample vitrification. Frozen samples were stored in liquid nitrogen until EM imaging in a Philips CM200FEG microscope operating at 200 kV and equipped with a TVIPS TemCam-F224HD CCD camera and a Gatan 626 Cryo-Holder.

2.8.2. Immunoblotting

Cells were recovered by centrifugation and pellets were lysed in RIPA buffer (50 mM Tris-HCl pH 8, 150 mM NaCl, 1% (v/v) NP-40, 0.1% (w/v) SDS, 0.5% (w/v) sodium deoxycholate) in the presence of protease inhibitor mixture. Insoluble material was removed by centrifugation at 13,000 g for 10 min at 4 °C.

Aliquots of cell lysates (20–30 μg proteins) or EVs (2–5 μg proteins) were mixed with sample buffer 5X (1 M Tris-HCl pH 6.8, 5% (w/v) SDS, 6% (v/v) glycerol, 0.01% (w/v) Bromophenol blue) containing 125 mM DTT. Samples were electrophoresed on 10–12% acrylamide gels and electrotransferred to PVDF membranes. After blocking, membranes were incubated overnight with the following primary antibodies: anti-CD9 (Santa Cruz, Dallas, USA), anti-β-actin (Sigma-Aldrich), anti-calnexin (Santa Cruz), anti-flotillin (BD Biosciences, Franklin Lakes, USA), anti-CD81 (Santa Cruz). HRP-linked secondary antibodies (GE Biosciences, Piscataway, USA) were probed according to manufacturer's instructions. Immunoblots were detected by chemiluminescence using ECL system (GE Biosciences).

2.9. Immunoblot detection of carbonylated proteins in control and CSE-treated cells, and released EVs

Levels of carbonylated proteins in cells and EVs were evaluated by indirect on-PVDF membrane protein labelling with 2,4-dinitrophenylhydrazine (DNPH) according to Colombo et al. (2016). Control or 1% CSE-treated cells were lysed in RIPA buffer as reported above. Aliquots of cell lysates (25 μg proteins) or EVs (18 μg proteins) were subjected to SDS-PAGE (10% acrylamide gels) and proteins were transferred onto a PVDF membrane. Membrane was washed for 15 min in PBS-T and incubated in 2 N HCl for 5 min before the derivatization step. PVDF membrane was incubated for 5 min in 0.1 mg/mL DNPH solution in 2 N HCl to derivatize protein carbonyls. After washing and blocking steps, the membrane was incubated with anti-DPN antibody (Molecular Probes, Eugene, OR, USA) to specifically bind to DNPH-labeled electroblotted proteins. Anti-rabbit HPR-coniugated were used as secondary antibodies (Cell Signalling, Beverly, USA). Immunoreactive proteins were finally evidenced by chemiluminescence using the ECL system. Film images were then acquired using a GS-800 imaging systems scanner (Biorad, Hercules, USA). After immunoblotting, PVDF membranes were stained with R-250 blu Coomassie according to Goldman et al. (2016), in order to define the total protein content of each lane. The carbonyl levels and the total protein levels were densitometrically defined using the software Quantity One (Biorad). The ratio between the optical density (OD) of each whole lane in the films and the OD of corresponding whole lane in the Coomassie-stained membranes were reported as levels of carbonylated proteins.

2.10. Lipid characterization and phospholipid fatty acid analysis of control and CSE-treated cells, and released EVs

2.10.1. Lipid extraction and characterization

The work up of the samples followed the previously published procedures (Ferreri et al., 2020; Küçüksayan et al., 2022). Briefly, 3×10^6 cells were added with tri-distilled H_2O (1 mL) and centrifuged at 10,000 x g for 15 min at 4 °C to obtain membrane pellet. They were then reconstituted in tri-distilled H_2O (1 mL); one aliquot (20 μl) was injected in the HPLC instrument (Agilent 1200, Santa Clara, USA) equipped with RP18 column (Macherey-Nagel EC 150/4.6, Nucleodur C18 HTEC, 5 μm) applying previously published calibration procedures and separation protocol (Ferreri et al., 2020; Küçüksayan et al., 2022), while the remaining part was extracted with $CHCl_3$/MeOH (2:1, v/v) (4 ×2 mL) according to the Folch method (Folch et al., 1957). The organic layers were collected, dried on anhydrous Na_2SO_4 and evaporated to dryness; the extracts (0.4–0.6 mg in each sample) were also checked by three different TLC analytical conditions (n-hexane/Et_2O 9:1 v/v, n-hexane/Et_2O 3:7 v/v and $CHCl_3$/MeOH/H_2O 4.3:2.3:0.2 v/v/v) evidencing the presence of phospholipids and free cholesterol. The lipid extracts were then added with 0.5 M KOH in MeOH (0.5 mL) for the conversion to Fatty Acid Methyl Esters (FAME). The transesterification reaction was left stirring for 10 min and quenched by brine (0.5 mL); FAME were extracted with n-hexane (4 × 2 mL), dried on anhydrous Na_2SO_4, evaporated to dryness and dissolved in n-hexane (10 μl) for GC analysis using standard references for peak identification and quantitation as described in the next section and in previous work (Sansone et al., 2013; Scanferlato et al., 2019).

EV samples (100 μg) were treated as previously described for HPLC and GC analyses of the lipid and fatty acid contents, respectively (Ferreri et al., 2020).

2.10.2. Fatty acid methyl ester analysis by gas chromatography

Gas chromatography and detection with a flame ionization detector (GC-FID) were carried out by Agilent 6850 equipment (Agilent, Milan, Italy) in splitless mode using a 60 m × 0.25 mm × 0.25 μm (50%-cyanopropyl)-methylpolysiloxane column and the following oven program: temperature started from 165 °C, held for 3 min, followed by an increase of 1 °C/min up to 195 °C, held for 40 min, followed by a second increase of 10 °C/min up to 240 °C, and held for 10 min. A constant pressure mode (29 psi) was chosen with helium as the carrier gas. FAME obtained from membrane phospholipids (see above) were separated and quantified using previously published procedures and commercially available standard references (Sansone et al., 2013; Scanferlato et al., 2019). FAME are expressed as relative percentage (mean ± SD) of the quantitative values of each fatty acid obtained by calibration curves calculated directly by the software Chem Station Agilent of the GC instrument. The recognized FAMEs corresponded to > 99% of the peaks present in the GC run. The procedures for LOD, LOQ and calibration of GC instrument have been previously detailed (Sansone et al., 2013; Scanferlato et al., 2019).

Dimethyl disulphide adducts of FAME were analyzed by GC-MS (Thermo Scientific Trace 1300) equipped with a 15 m × 0.25 mm × 0.25 μm 5% phenyl methyl polysiloxane column (Thermo Scientific™ TraceGOLD™ -SQC) with helium as the carrier gas, coupled to a mass-selective detector (Thermo Scientific ISQ, Waltham, MA, USA) with the following oven program: temperature started at 80 °C, maintained for 2 min, increased at a rate of 15 °C/min up to 140 °C, increased at a rate of 5 °C/min up to 280 °C and held for 10 min

The results of the FAME profiles in cell membrane are listed in

Table 1
Fatty acid residues (as fatty acid methyl esters, calculated as % rel. quant.) and corresponding fatty acid indexes of control and 1% CSE-treated cells.

FAME (% rel. quant)[1]	CTRL (n = 8)	1% CSE (n = 8)
	mean±SD	mean±SD
14:0	1.22 ± 0.39	0.96 ± 0.43
16:0	24.52 ± 3.11	22.72 ± 5.45
6 *cis* 16:1	3.33 ± 0.35	3.00 ± 0.50
7 cis 16:1	traces	traces
9 *cis* 16:1	1.48 ± 0.32	1.44 ± 0.31
18:0	14.12 ± 1.34	13.80 ± 2.33
9 trans 18:1	0.18 ± 0.06	0.20 ± 0.04
8 *cis* 18:1	2.70 ± 0.51	2.86 ± 0.92
9 *cis* 18:1	29.37 ± 2.76	30.60 ± 4.33
11 *cis* 18:1	6.33 ± 0.92	6.46 ± 1.11
5, 8 *cis* 18:2	0.30 ± 0.08	0.38 ± 0.11
mono*trans*18:2	0.13 ± 0.02	0.17 ± 0.10
18:2 n-6	1.93 ± 0.73	1.84 ± 0.69
20:0	0.21 ± 0.09	0.37 ± 0.13 *
11 *cis* 20:1	0.39 ± 0.06	0.44 ± 0.06
20:3 n-6, DGLA	0.98 ± 0.21	1.08 ± 0.23
20:4 n-6, ARA	5.41 ± 0.96	5.99 ± 1.11
mono*trans* ARA	0.11 ± 0.02	0.15 ± 0.05
20:5 n-3, EPA	0.54 ± 0.10	0.49 ± 0.18
22:5 n-3, DPA	1.60 ± 0.47	2.08 ± 0.86
22:6 n-3, DHA	3.91 ± 0.80	4.11 ± 1.38
SFA	40.06 ± 4.24	37.85 ± 7.92
MUFA	44.45 ± 4.24	45.47 ± 6.26
PUFA	14.68 ± 2.31	15.97 ± 3.06
n-6	8.32 ± 1.25	8.91 ± 1.14
n-3	6.05 ± 1.24	6.68 ± 2.22
n − 6/n- 3	1.40 ± 0.19	1.44 ± 0.42
SFA/MUFA	0.92 ± 0.18	0.87 ± 0.30
total *trans*	0.41 ± 0.07	0.52 ± 0.12*
n-10	6.33 ± 0.71	6.23 ± 0.89
ARA/EPA	10.18 ± 1.44	13.59 ± 5.0
PI	70.76 ± 12.90	77.43 ± 20.04

[1] Values are obtained in μg/mL considering the GC peak areas recognized and calibrated with standard references (corresponding to >99% of the total peaks of the chromatogram). Values are expressed in percentages relative to the sum of all the quantities of the recognized peaks ± SD (% rel. quant.) from the analyses of n = 8 samples. Table reports also the distribution of fatty acids grouped on the basis of their unsaturation level, the content of n-3 e n-6 PUFA and of *trans* geometrical isomers of unsaturated fatty acids (*$p \leq 0.04$, CSE-treated cells *vs* CTRL). SFA, Saturated Fatty Acids; MUFA, Mono-Unsaturated Fatty Acids; PUFA, Poly-Unsaturated Fatty Acids; n-6 PUFA (n-6); n-3 PUFA (n-3); PI = [(MUFA TOT) + (C18:2) + (C20:3) + (C20:4) + (C20:5) + (C22:6)].

Table 1. A representative example of GC chromatogram of the analyzed cell sample is reported in Fig. 1 S. The fatty acid composition of EVs is listed in Table 2.

2.10.3. DMDS derivatization

The FAME mixtures were also treated by DMDS derivatization and GC/MS analysis for the unambiguous assignment of the double bond position as previously described (Sansone et al., 2013; Scanferlato et al., 2019).

2.11. Determination of protein concentration

The protein concentration was determined spectrophotometrically by Bradford method using Bio-Rad protein assay. Bovine serum albumin was used to generate standard curve.

2.12. Statistical analysis

All data are expressed as mean ± SD (standard deviation). Statistical analysis was performed using GraphPad Prism 5.0 software (GraphPad Software, Inc., San Diego, CA, USA). We used the non-parametric unpaired t-test, two-tailed, with a 95% confidence interval when 2 groups were compared, whereas analysis of variance (ANOVA) with Bonferroni correction were used for multiple pairwise comparisons. p-values below 0.05 were considered statistically significant.

3. Results

3.1. CSE exposure decreased viability and increased intracellular levels of ROS and carbonylated proteins in BEAS-2B cells

Firstly, we evaluated the relative survival and the intracellular levels of ROS in BEAS-2B cells exposed to various CSE concentrations (0.5–10%), that were chosen on the basis of previous studies on the same cell line (Gornati et al., 2013; Colombo et al., 2019). As shown in Fig. 1, CSE reduced viability (panel A) and increased ROS levels (panel B) in a dose-dependent manner in BEAS-2B cells.

Then, we evaluated levels of carbonylated proteins, which are stable markers of protein oxidation, in BEAS-2B cells incubated in the absence (CTRL) or presence of various CSE concentrations (0.5–5%). As reported in Fig. 2, CSE increased intracellular levels of carbonylated proteins in a dose-dependent manner. In addition, we evaluated the levels of malondialdehyde (MDA), which is a well-known product of lipid peroxidation, in cells exposed for 24 h to various CSE concentrations (0.5–10%). Only the highest concentration of CSE was able to significantly increase MDA levels (data not shown).

3.2. Characterization of EVs released by control and CSE-treated cells

EVs were isolated from culture media of BEAS-2B cells incubated in the absence (CTRL-EVs) or presence of 1% CSE (CSE-EVs), a concentration that only slightly affect cell viability but increased the intracellular levels of ROS and carbonylated proteins (see Figs. 1 and 2). EVs, isolated by differential centrifugation, were characterized by SEM, NTA, cryo-TEM and immunoblotting. SEM images showed the presence of round cup-shaped vesicles typical of exosomes and/or small plasma membrane-derived microvesicles, both in CTRL-EVs and CSE-EVs (Fig. 3A). Cryo-TEM revealed that our preparations contained round shaped vesicles surrounded by membrane bilayer (Fig. 3B). The mean concentration (particles/mL ± SD) and size distribution of EV populations isolated from cell culture media of CTRL and CSE-treated cells were measured by NTA. No significant differences in EV concentrations were observed between CTRL and CSE samples (Fig. 3C). Most of the EVs from CTRL and CSE-treated cells had an average size of 123 + 1.1 and 125.6 + 1.2 nm (with a mode size 93.6 +5.8 and 87.5 +2.5), respectively (Fig. 3C). Immunoblotting showed the presence in our vesicle preparations of EV markers such as CD81, CD9 and flotillin-1, whereas calnexin (marker of endoplasmic reticulum) and actin were not detected (Fig. 3D). These results indicated that our EV preparations were devoid of endoplasmic reticulum or cytoskeletal components and were enriched of vesicles having a size typical of small EVs (Kowal et al., 2016; Théry et al., 2018).

3.3. Carbonylated protein levels and fatty acid profiles in EVs released by control and CSE-treated cells

In this section, results regarding the specific molecular cargo of EVs released by control and CSE-treated cells have been reported. In particular, we evaluated if CSE exposure modify the content of oxidized proteins and alter the phospholipid fatty acid composition of EVs released by BEAS-2B cells. As shown in Fig. 4, CSE-EVs presented higher content of carbonylated proteins, compared to CTRL-EVs. In order to unambiguously confirm the presence of carbonylated proteins in CSE-EVs, we also tested an EV-enriched fraction obtained by loading EVs recovered by the last step of differential ultracentrifugation on the top of an qEV/70 nm SEC column. Western blotting of the SEC fractions

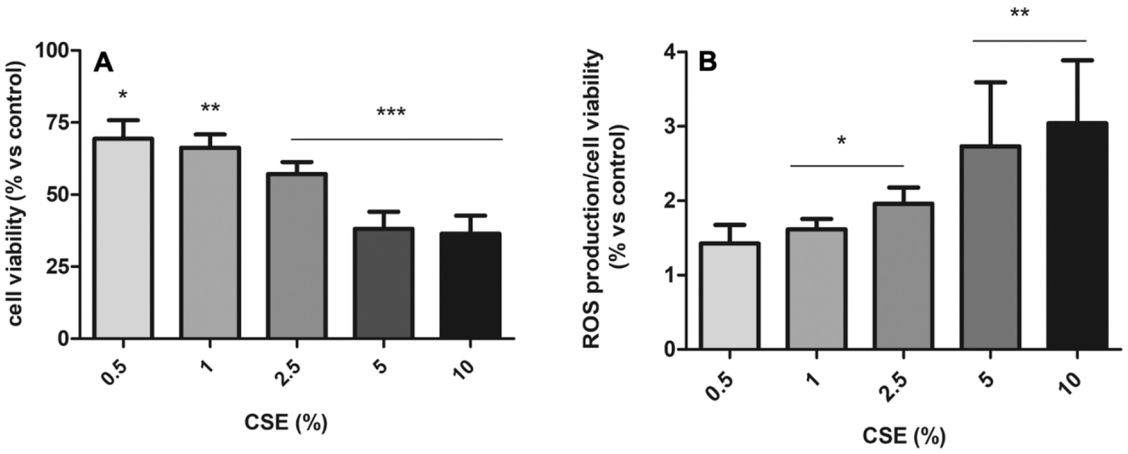

Fig. 1. Cell viability and intracellular ROS levels in BEAS-2B cells exposed to various CSE concentrations. Cells were treated for 24 h with CSE at the indicated concentrations. A) Cell viability was evaluated using MTT assay. Results are expressed as percentage of cell survival compared with control (*$p < 0.05$, **$p < 0.001$, ***$p < 0.0001$, CSE-treated cells *vs* controls). B) Intracellular ROS production was evaluated using the H_2DCFDA assay. Normalized DCF fluorescence values are expressed as percentage compared with control (*$p < 0.05$, **$p < 0.001$, CSE-treated cells *vs* controls). All data are reported as mean ± S.D. from four independent experiments carried out in triplicate.

Table 2
Fatty acid residues (as fatty acid methyl esters, calculated as % rel. quant.) and corresponding fatty acid indexes of EVs released by control and CSE-treated cells.

FAME (% rel. quant)[1]	CTRL-EVs (n = 8)	CSE-EVs (n = 6)
	means±SD	means±SD
14:0	1.89 ± 0.28	1.66 ± 0.43
16:0	26.31 ± 1.98	28.52 ± 1.13*
6 *cis* 16:1	3.14 ± 0.38	2.21 ± 0.24* **
7 cis 16:1	traces	traces
9 *cis* 16:1	1.48 ± 0.55	1.48 ± 0.36
18:0	19.57 ± 2.51	21.19 ± 0.76
9 trans 18:1	0.08 ± 0.02	0.07 ± 0.01
8 *cis* 18:1	2.19 ± 0.47	2.25 ± 0.33
9 *cis* 18:1	23.11 ± 1.69	20.29 ± 1.72* *
11 *cis* 18:1	3.90 ± 0.85	3.70 ± 0.58
5, 8 *cis* 18:2	0.17 ± 0.02	0.14 ± 0.05
mono*trans*18:2	0.07 ± 0.02	0.06 ± 0.02
18:2 n-6	2.50 ± 0.68	3.03 ± 0.17
20:0	1.69 ± 0.31	2.01 ± 0.10*
11 *cis* 20:1	0.43 ± 0.19	0.65 ± 0.05*
20:3 n-6, DGLA	0.90 ± 0.19	1.24 ± 0.24*
20:4 n-6, ARA	4.42 ± 0.33	4.11 ± 0.58
mono*trans* ARA	0.05 ± 0.03	0.08 ± 0.01
20:5 n-3, EPA	0.65 ± 0.16	0.79 ± 0.12
22:5 n-3, DPA	1.69 ± 0.70	1.49 ± 0.40
22:6 n-3, DHA	3.62 ± 0.94	3.15 ± 0.47
SFA	49.45 ± 3.77	53.37 ± 1.49*
MUFA	35.07 ± 2.52	31.62 ± 1.13* *
PUFA	13.95 ± 2.03	13.96 ± 1.45
n-6	7.82 ± 0.82	8.38 ± 0.76
n-3	5.96 ± 1.66	5.43 ± 0.70
n − 6/n- 3	1.31 ± 0.38	1.55 ± 0.11
SFA/MUFA	1.42 ± 0.21	1.69 ± 0.10*
total *trans*	0.20 ± 0.04	0.19 ± 0.02
n-10	5.50 ± 0.66	4.60 ± 0.42
ARA/EPA	7.46 ± 3.12	5.34 ± 1.39
PI	65.89 ± 11.78	61.65 ± 7.47

[1] Values are obtained in μg/mL considering the GC peak areas recognized and calibrated with standard references (corresponding to >99% of the total peaks of the chromatogram). Values are expressed in percentages relative to the sum of all the quantities of the recognized peaks ± SD (% rel. quant.) from the analyses of n = 8 CTRL-EVs and n = 6 CSE-EVs. Table reports also the distribution of fatty acids grouped on the basis of their unsaturation level, the content of n-3 e n-6 PUFA and of *trans* geometrical isomers of unsaturated fatty acids (*p ≤ 0.034, **p ≤ 0.009, ***p ≤ 0.0002, CSE-EVs *vs* CTRL-EVs). SFA, Saturated Fatty Acids; MUFA, Mono-Unsaturated Fatty Acids; PUFA, Poly-Unsaturated Fatty Acids; n-6 PUFA (n-6); n-3 PUFA (n-3); PI = [(MUFA TOT) + (C18:2) + (C20:3) + (C20:4) + (C20:5) + (C22:6)].

revealed the presence of the EV marker protein CD81 in the fraction 8 (Fig. 2S). EVs contained in this fraction were recovered by ultracentrifugation and analyzed for the presence of carbonylated proteins. Results showed that EVs from CSE-treated cells contained higher level of carbonylated proteins, compared to the control (Fig. 3S).

Then, we analyzed the phospholipid fatty acid composition of CTRL and 1% CSE-treated cells, and their released EVs. Cells and EVs were first examined for the lipid classes, identifying phosphatidylethanolamine (PE), phosphatidylserine (PS) and phosphatidylcholine (PC), together with cholesterol (CHO) and sphingomyelins (SM), by appropriate methods and standard references. In cells, treatment with 1% CSE induced a significant increase in the content of PS and a reduction in the content of PE (Fig. 5A), whereas an increased level of SM was observed in CSE-EVs compared to CTRL-EVs (Fig. 5B).

Then, the phospholipid fatty acid composition of cells and EVs was analyzed by GC. Tables 1 and 2 report the percentage of FAME from membrane phospholipids of cells and EVs, respectively. Tables reported also the positional and geometric isomers of unsaturated fatty acids and FAME grouped in saturated (SFA), monounsaturated (MUFA) and PUFA, as the phospholipid saturation degree determines important biophysical and functional properties of membranes.

In BEAS-2B cells, SFA represented ~40 % of total fatty acids whereas the content of MUFA and PUFA were ~45% and ~15%, respectively (Table 1). Regarding SFA, the most abundant fatty acids were palmitic (16:0) and stearic acid (18:0), whereas regarding MUFA ~6 % of them were represented by n-10 fatty acids. In particular, the analysis of MUFA positional isomers demonstrated that among the hexadecenoic fatty acid (16:1) family the most abundant species were sapienic acid (6 *cis*16:1-n10) followed by palmitoleic acid (9 *cis* 16:1 n-7), whereas in the 18:1 family the most abundant species were oleic acid (9 cis-18:1 n-9) followed by 11 *cis* 18:1 n-7 and 8 *cis*-18:1 n-10 (Table 1). The total *trans* fatty acid (TFA) isomers including MUFA, PUFA isomers, were ~0.4% (Table 1).

Treatment of BEAS-2B cells with 1% CSE induced only few changes in phospholipid fatty acid profiles consistent of higher levels of arachidic acid (20:0) and of the total content of TFA, compared to controls (Table 1).

In CTRL-EVs, SFA represented ~50% of total fatty acids whereas the content of MUFA and PUFA were ~35 % and 15 %, respectively (Table 2). As for cells, palmitic (C16:0) and stearic (C18:0) acids were the most abundant SFA in CTRL-EVs (Table 2). Regarding C16 and C18 positional MUFA, we observed that the most abundant isomer of 16:1 family is sapienic acid (6 cis16:1 -n10), whereas oleic acid (9 cis-18:1 n-9) was the most abundant isomer among 18:1 MUFA (Table 2). Focusing the attention on CSE-induced effects, we observed numerous rearrangements in the acyl chains of the membrane phospholipids of CSE-EVs, which presented significant higher content of palmitic (16:0) and arachidic (20:0) acids, and reduced levels of sapienic (6 cis-16:1 n-10) and oleic (9 cis-18:1 n-9) acids, compared to CTRL-EVs (Table 2). These changes accounted for the higher SFA levels and lower MUFA levels, resulting in a significant increase of the SFA/MUFA ratio in CSE-EVs (Table 2). Further, higher levels of 11cis-eicosenoic acid (11cis-20:1 n:9) and dihomo-γ-linolenic acid (20:3 n-6, DGLA) were observed in CSE-EVs, compared to CTRL-EVs (Table 2).

4. Discussion

Several studies have demonstrated that various cell types exposed to CSE release EVs having an altered biochemical cargo which might affect signaling and biological responses to other cells (Haque et al., 2020; Li et al., 2010; Benedikter et al., 2019). Even if the effects exerted by EVs released by airway epithelial cells treated with CSE have been investigated, few studies analyzed their molecular cargo.

Several evidences indicate that the exposure of BEAS-2B cells to CSE induces the release of EVs enriched in tissue factors *via* depletion of cell surface thiols (Stassen et al., 2019) and in proteins involved in haemostasis, cell communication and signal transduction (Benedikter et al., 2019). Corsello and coworkers (2019) demonstrated that human small airway epithelial cells (SAE) treated with cigarette smoke condensate release EVs displaying an enrichment in hsa-miR-3913–5p, whose potentially target genes are involved in lipid transport, lipid binding, and regulation of mRNA stability.

Most of the effects exerted by CSE have been linked to its pro-oxidant components that can induce oxidative stress and consistently can affect EV release and composition, enriching their cargo in oxidized molecules (Chiaradia, 2021).

In the present study, we demonstrated that 24 h treatment of BEAS-2B cells with 1% CSE increased the content of carbonylated proteins not only in cells but also in their released EVs. Furthermore, relevant differences in phospholipid fatty acid composition of CSE-EVs have been observed, whereas only few changes were observed in the fatty acid asset of membrane phospholipids of CSE-treated cells.

In the first part of this study, we demonstrated that CSE reduced viability of BEAS-2B cells and elevated intracellular ROS levels, in a dose-dependent manner. These results are in agreement with other studies that suggest a crucial role of ROS and oxidative cell injury in the smoking-associated pathology of airway tissues (Van Der Toorn et al.,

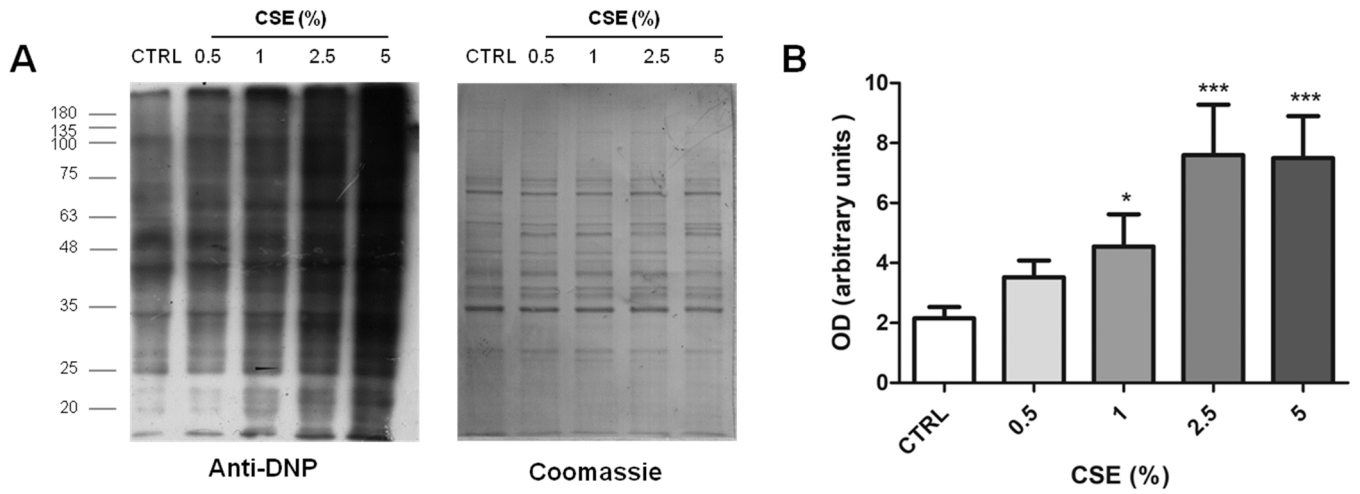

Fig. 2. Protein carbonylation levels in BEAS-2B cells treated with various CSE concentrations. Cells were treated for 24 h with CSE at the indicated concentrations. A) Representative immunoblot of carbonylated proteins and the corresponding Coomassie-stained PVDF membranes. B) Bar graph reports carbonylated protein levels expressed as ratio of optical density (OD) obtained from the whole lane on film and the OD of the corresponding lane in Coomassie-stained PVDF membrane (*p < 0.05; ***p < 0.001, CSE-treated cells *vs* CTRL, n = 4).

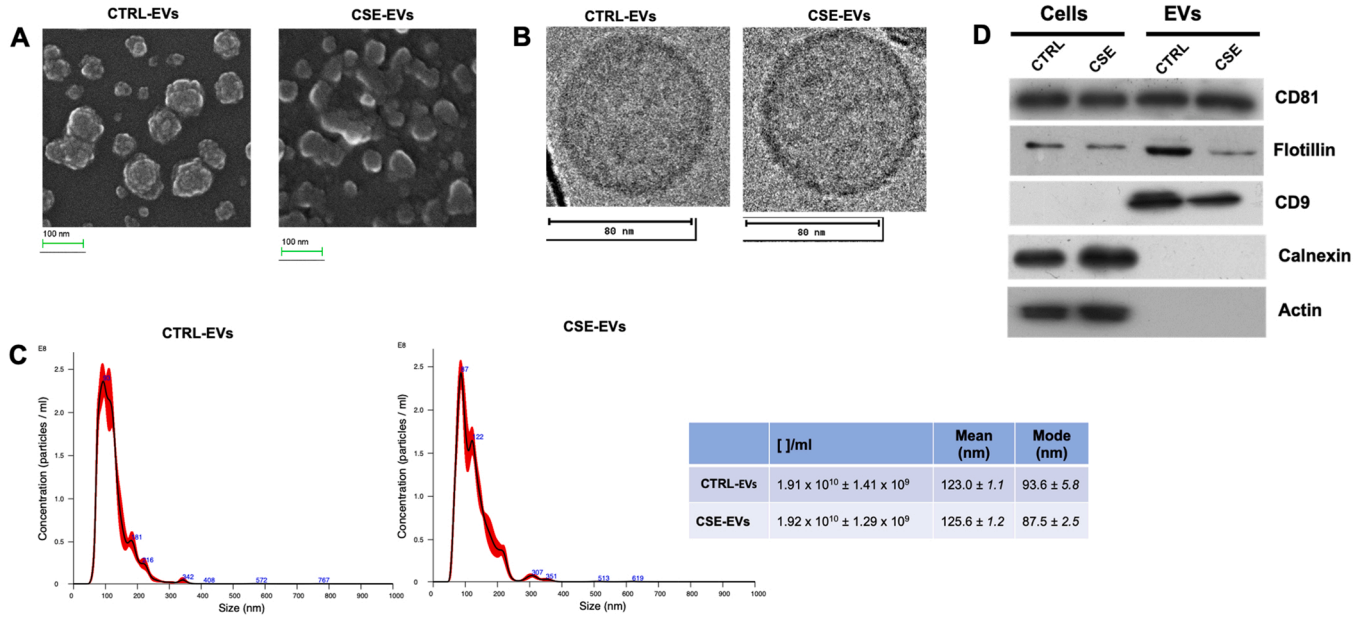

	[ ]/ml	Mean (nm)	Mode (nm)
CTRL-EVs	1.91 x 10^{10} ± 1.41 x 10^{9}	123.0 ± *1.1*	93.6 ± *5.8*
CSE-EVs	1.92 x 10^{10} ± 1.29 x 10^{9}	125.6 ± *1.2*	87.5 ± *2.5*

Fig. 3. Characterization of EVs released from control and CSE-treated cells. EVs were isolated from cell culture media of control (CTRL-EVs) and 1% CSE-treated cells (CSE-EVs), as described in Materials and Methods. A) Representative images of EVs by SEM. B) Representative cryo-TEM images of EVs. C) Concentration and size distribution of the released EVs by NTA. Representative distribution is shown. Number of particles/mL ([]/mL), mean (nm) and mode (nm) are reported in the Table. Data are expressed as mean ± SD of five measurements. D) Cell lysates and EVs were separated by SDS-PAGE, electro-transferred and probed with the indicated positive and negative EV markers. Immunoblots are representative of two independent experiments.

2009; Reis et al., 2021). We also observed a dose-dependent increase of carbonylated protein levels in CSE-treated cells, compared to controls. Similar results were obtained by Colombo et al. (2019) by exposing a human bronchial epithelial cell line (16-HBE cells) to 2.5–10% CSE for 1 h, 3 h and 24 h. However, our results showed increased intracellular levels of carbonylated proteins also at 1% CSE, a concentration able to induce oxidative stress without a remarkable reduction of cell viability. It is well known that carbonylated proteins completely or partially lose their function until they become toxic for cells. In addition, they cannot be efficiently removed by the proteasome ubiquitin system. In particular, Kästle and co-workers demonstrated that carbonylated proteins are not preferentially ubiquitinated (Kästle and Grune, 2011; Kästle et al., 2012), whereas Colombo et al. (2019) observed a reduction of protein carbonylation levels after 24 h, compared to 1 h and 3 h of CSE exposure of 16-HBE cells, without significant differences in protein ubiquitination. Since EVs can also act in removing intracellular unwanted material (Chiaradia, 2021; Tancini et al., 2019), carbonylated proteins loaded in EVs could represent an additional way to dispose of oxidatively damaged proteins, in order to avoid their detrimental intracellular overload.

In the present study, we isolated EVs released by control or 1% CSE-exposed cells and investigated their cargo. CTRL-EVs and CSE-EVs are both round shaped vesicles surrounded by a membrane bilayer. SEM and NTA analyses showed no significant differences in morphology and size distribution between CTRL-EVs and CSE-EVs. Interestingly, we did not observe an increased EV release by 1% CSE-treated BEAS-2B, in

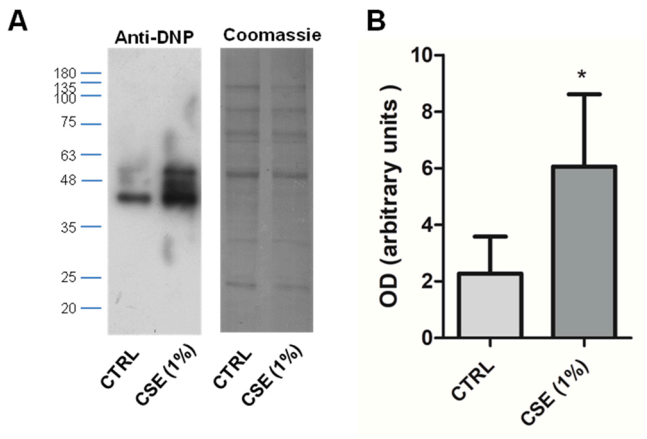

Fig. 4. Protein carbonylation levels in EVs released by control and CSE-treated cells. EVs were isolated from cell culture media of control (CTRL) and 1% CSE-treated cells, as described in Materials and Methods. A) Representative immunoblot of carbonylated proteins and the corresponding Coomassie-stained PVDF membranes. B) Bar graph reports carbonylated protein levels expressed as ratio of optical density (OD) obtained from the whole lane on film and the OD of the corresponding lane in Coomassie-stained PVDF membrane (* $p < 0.025$, $n = 4$).

accordance with other authors (Fujita et al., 2015; Stassen et al., 2019). Conversely, the increased secretion of EVs from cultured human bronchial epithelial cells exposed to CSE has been reported in some studies (Saxena et al., 2021; Benedikter et al., 2017; Moon et al., 2014). This discrepancy could be due to differences in CSE concentration used in the studies, as only concentrations > 1% CSE seems to be able to increase the release of EVs (Saxena et al., 2021; Benedikter et al., 2017; Moon et al., 2014; Stassen et al., 2019). However, in our model, concentrations of CSE > 1% were associated with a significant decrease in cell viability. Interestingly, oxyblot analyses showed that 24 h treatment of BEAS-2B cells with 1% CSE increased the content of oxidatively modified proteins, not only in cells but also in their released EVs, indicating that the exposure of BEAS-2B cells to low CSE concentrations is able to alter the composition of EVs without affecting the level of EV release. However, the effects of oxidative stimuli on proteins might be related to the cell type and oxidative conditions. For instance, Eldh's (2010) study evidenced that 24 h exposure of mouse mast cell line (MC/9) to H_2O_2 (125 mM) increases the level of oxidized proteins in cells, but not in exosomes. However, the presence of carbonylated proteins has been evidenced in the EVs derived from pigmented ciliary epithelium cells under oxidative stress condition induced by 2,2–Azobis (2–amidinopropane) dihydrochloride (Lerner et al., 2020).

Lipid extraction and characterization by GC analyses of phospholipid fatty acid composition in CSE-EVs and CTRL-EVs, evidenced interesting differences, whereas only a few changes were observed in the phospholipid fatty acid asset of CSE-treated cells. These data indicate that the analysis of EV lipid asset, can highlight differences between control and CSE-treated samples that did not emerge from the analysis of the cellular counterparts. Cells exposed to 1% CSE presented a significant increase in arachidic acid (20:0) and TFA isomers, compared to controls. It is well known that the *cis* configuration of the double bonds of unsaturated fatty acids is the most abundant configuration present in membrane phospholipids. Oxidative stress conditions can cause isomerization of unsaturated fatty acids from the natural *cis* to unnatural *trans* configuration (Ferreri et al., 2016, 2022), which is the thermodynamically most favored structure. By increasing free radicals, smoke can contribute to biomolecule reactivity and TFA isomer formation, as reported for *trans*-arachidonic acid isomers detected in human blood plasma of smokers (Hung et al., 2016). The presence of TFA in cell membrane phospholipids can influence physical and functional properties of the membrane, such as fluidity, permeability and cell signaling (Cort et al., 2016). Besides, *cis-trans* isomerization is a process that can amplify the reactivity of relatively small quantities of radical species generated in the biological environment. Therefore, the mild oxidative stress induced by 1% CSE might be sufficient to induce *cis-trans* isomerization of the double bond of unsaturated fatty acids, whereas does not produce extensive lipid peroxidation, as demonstrated by the lack of increase of MDA levels in treated cells (data not shown). Our result indicates that the evaluation of *trans* geometrical isomers in cell membranes could be a useful indicator of an early stage of oxidative stress-induced cell damage. It is important to add that the detection of TFA, as well as of the positional isomers for purposes of precision medicine, requires the use of GC under specific conditions of column length and oven program, as reported in the Materials and Methods. This is the gold standard methodology to separate geometrical as well as positional isomers, whereas the sole use of direct injection of lipid mixture in mass spectrometry cannot give precise quantifications of small amounts of such isomers, especially when they are in mixture with other fatty acids such as in biological samples.

Interestingly, the quantification of lipid classes by HPLC revealed that CSE treatment caused changes in the cellular phospholipid composition, with a decrease of PE and an increase of PS, which is

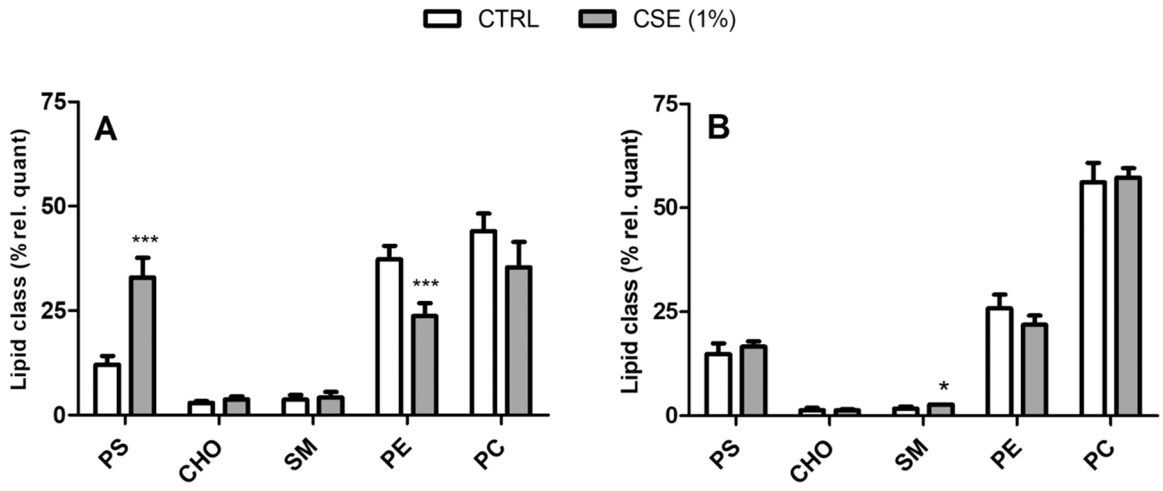

Fig. 5. Main lipid classes isolated from control and CSE-treated cells (A), and their corresponding EVs (B). Values are expressed as relative quantitative percentages (% rel. quant.) calculated from the quantities of lipids obtained by HPLC analysis identified and calibrated by the standard references. Values are mean ± SD of experiments performed in replicates (***$p \leq 0.0005$ (1% CSE-treated cells *vs* controls, $n = 8$) (*$p \leq 0.05$, CSE-EVs *vs* CTRL-EVs, $n = 8$ and $n = 6$, respectively). PS = phosphatidylserine, CHO = free cholesterol; PE = phosphatidylethanolamine; SM = sphingomyelin; PC = phosphatidylcholine.

known to play a pivotal role in apoptotic signaling (Barth et al., 2017).

Regarding fatty acids composition of released EVs, in line with previous studies (Llorente et al., 2013; Sagini et al., 2018a; Ferreri et al., 2020; Buratta et al., 2021), we observed an enrichment in the content of SFA and MUFA, compared to parental cells. The SFA enrichment can contribute to membrane rigidity of EVs (Llorente et al., 2013; Trajkovic et al., 2008) as well as to EV stability in biological fluids (Alvarez-Erviti et al., 2011). Besides, CSE exposure affected the fatty acid composition of EV more than cells. The most relevant changes in CSE-EVs were the increased content of palmitic acid (16:0) and arachidic acid (20:0) and the reduced levels of sapienic acid (6 cis-16: 1 n-10), oleic acid (9 cis-18: 1 n-9) and 11cis-eicosenoic acid (11cis-20:1 n:9), which lead to an increase in the SFA/MUFA ratio. This can suggest a metabolic shift induced by CSE, with a decreased desaturase enzymatic conversion of SFA into MUFA. Indeed, in THP-1 cells cigarette smoke induced a reduction of desaturase activity, which modified linoleic acid and the omega-6 PUFA biosynthetic pathway (Ghezzi et al., 2007). Moreover, it has been demonstrated that SFA-enriched EVs induce pro-inflammatory responses in target cells (Kakazu et al., 2016; Hirsova et al., 2016) and that saturation level of membrane phospholipids influence EV uptake by recipient cells (Buratta et al., 2021). The only significant difference on PUFA components of EVs was found to be the level of omega-6 DGLA (20:3 n-6) that increases in CSE-EVs, compared to CTRL-EVs. DGLA, one of the downstream omega-6 PUFAs derived from linoleic acid, is the precursor for series-1 lipid mediators, but it is also the precursor of arachidonic acid through the delta-5 desaturase transformation (Wang et al., 2012). This increase suggests a desaturase impairment caused by CSE. Thus, CSE-treated cells released EVs enriched in phospholipid containing DGLA which might be converted in bioactive lipids in target cells. Notably, EVs carry and deliver membrane-derived bioactive lipids protecting them from degradation and play a role in their transcellular synthesis (Sagini et al., 2018b). Lipid analysis revealed that CSE-EVs are enriched in SM, probably linked to the SFA enrichment observed in the fatty acid families.

5. Conclusion

The present study expands the knowledge about the biochemical cargo of EVs released by airway epithelial cells exposed to CSE. Overall, our results demonstrate that cell treatment with 1% CSE induced the release of EVs with altered phospholipid fatty acid composition, and an increased cargo of carbonylated proteins. The release of oxidatively modified proteins *via* EVs might represent a mechanism used by cells to remove toxic proteins in order to maintain cell homeostasis. On the other hand, EVs containing oxidized proteins can induce harmful effects in target cells such as inflammatory responses. The further identification of specific oxidized protein species in CSE- EVs will be useful to predict the effects exerted by CSE-EVs on neighboring or distant target cells. Regarding lipid composition, the increased SFA/MUFA ratio observed in CSE-EVs might influence their biological and targeting properties. Therefore, getting insights into the molecular composition of EVs will be useful to predict their biological effects, as it has been demonstrated that cells exposed to CSE-EVs undergo pro-inflammatory and pro-fibrotic changes. The same predictivity can be foreseen for the TFA presence that has been detected in cell membrane phospholipids, confirming cis-trans isomerization as first indicator of changes induced by the smoke habits. Results of the present *in vitro* study could be a starting point for the utilization of circulating EVs and, in particular their oxidized protein cargo and SFA/MUFA ratio, as biomarkers for the diagnosis of CS-induced lung damage and/or CS-related diseases.

CRediT authorship contribution statement

Conceptualization, SB, EC and CE; designed experiments, SB, EC, CF; cell treatments and EV isolation, RL, GC and RMP; oxyblot, AT; lipid analysis, AS, CF; SEM analysis, SG; writing-original draft preparation, SB, EC, BT; tables and figures, AS, SB, EC; statistical analysis and data processing, EC, CF and AS; writing—review and editing, AG, MD, LU, CE. All authors reviewed and critically revised the paper.

Declaration of Competing Interest

The authors declare no competing interests.

Data Availability

No data was used for the research described in the article.

Acknowledgements

This work was supported by University of Perugia, Grant Fondo d'Ateneo per la Ricerca di BASE 2017–2019 to Elisabetta Chiaradia and Grant Fondo d'Ateneo per la Ricerca di BASE 2021 to Sandra Buratta (RICBASE2021BURATTA).

The authors would like to thank Prof. Pietro Lupetti and the team of the Electron Microscopy Facility, Department of Life Sciences, University of Siena (Italy), for cryo-electron microscopy analyses.

Appendix A. Supporting information

Supplementary data associated with this article can be found in the online version at doi:10.1016/j.ejcb.2022.151285.

References

Abels, E.R., Breakefield, X.O., 2016. Introduction to extracellular vesicles: biogenesis, RNA cargo selection, content, release, and uptake. Cell. Mol. Neurobiol. 36, 301–312. https://doi.org/10.1007/s10571-016-0366-z.

Alvarez-Erviti, L., Seow, Y., Yin, H., Betts, C., Lakhal, S., Wood, M.J., 2011. Delivery of siRNA to the mouse brain by systemic injection of targeted exosomes (https://doi:). Nat. Biotechnol. 29, 341–345. https://doi.org/10.1038/nbt.1807.

Barth, N.D., Marwick, J.A., Vendrell, M., Rossi, A.G., Dransfield, I., 2017. The "phagocytic synapse" and clearance of apoptotic cells (https://doi:). Front. Immun. 8, 1708. https://doi.org/10.3389/fimmu.2017.01708.

Benedikter, B.J., Wouters, E.F.M., Savelkoul, P.H.M., Rohde, G.G.U., Stassen, F.R.M., 2018. Extracellular vesicles released in response to respiratory exposures: implications for chronic disease. J. Toxicol. Environ. Health B Crit. Rev. 221, 142–160. https://doi.org/10.1080/10937404.2018.1466380.

Benedikter, B.J., Volgers, C., van Eijck, P.H., Wouters, E.F.M., Savelkoul, P.H.M., Reynaert, N.L., Haenen, G.R.M.M., Rohde, G.G.U., Weseler, A.R., Stassen, F.R.M., 2017. Cigarette smoke extract induced exosome release is mediated by depletion of exofacial thiols and can be inhibited by thiol-antioxidants. Free Radic. Biol. Med. 108, 334–344. https://doi.org/10.1016/j.freeradbiomed.2017.03.026.

Benedikter, B.J., Bouwman, F.G., Heinzmann, A.C.A., Vajen, T., Mariman, E.C., Wouters, E.F.M., Savelkoul, P.H.M., Koenen, R.R., Rohde, G.G.U., van Oerle, R., Spronk, H.M., Stassen, F.R.M., 2019. Proteomic analysis reveals procoagulant properties of cigarette smoke-induced extracellular vesicles. J. Ext. Ves. 8, 1585163. https://doi.org/10.1080/20013078.2019.1585163.

Buratta, S., Urbanelli, L., Sagini, K., Giovagnoli, S., Caponi, S., Fioretto, D., Mitro, N., Caruso, D., Emiliani, C., 2017. Extracellular vesicles released by fibroblasts undergoing H-Ras induced senescence show changes in lipid profile. PLoS One 12, e0188840. https://doi.org/10.1371/journal.pone.0188840.

Buratta, S., Shimanaka, Y., Costanzi, E., Ni, S., Urbanelli, L., Kono, N., Morena, F., Sagini, K., Giovagnoli, S., Romani, R., Gargaro, M., Arai, H., Emiliani, C., 2021. Lipotoxic stress alters the membrane lipid profile of extracellular vesicles released by Huh-7 hepatocarcinoma cells. Sci. Rep. 11, 4613. https://doi.org/10.1038/s41598-021-84268-9.

Chiaradia, E., Tancini, B., Emiliani, C., Delo, F., Pellegrino, R.M., Tognoloni, A., Urbanelli, L., Buratta, S., 2021. Extracellular vesicles under oxidative stress conditions: biological properties and physiological roles. Cells 10, 1763. https://doi.org/10.3390/cells10071763.

Colombo, G., Clerici, M., Garavaglia, M.E., Giustarini, D., Rossi, R., Milzani, A., Dalle-Donne, I.A., 2016. A step-by-step protocol for assaying protein carbonylation in biological samples. J. Chromatogr. B Anal. Technol. Biomed. Life Sci. 1019, 178–190. https://doi.org/10.1016/j.jchromb.2015.11.052.

Colombo, G., Garavaglia, M.L., Astori, E., Giustarini, D., Rossi, R., Milzani, A., Dalle Donne, I., 2019. Protein carbonylation in human bronchial epithelial cells exposed to cigarette smoke extract. Cell Biol. Toxicol. 35, 345–360. https://doi.org/10.1007/s10565-019-09460-0.

Corsello, T., Kudlicki, A.S., Garofalo, R.P., Casola, A., 2019. Cigarette smoke condensate exposure changes RNA content of extracellular vesicles released from small airway epithelial cells. Cells 8, 1652. https://doi.org/10.3390/cells8121652.

Cort, A., Ozben, T., Melchiorre, M., Chatgilialoglu, C., Ferreri, C., Sansone, A., 2016. Effects of bleomycin and antioxidants on the fatty acid profile of testicular cancer cell membranes (https://doi:). Biochim. Biophys. Acta 1858, 434–441. https://doi.org/10.1016/j.bbamem.2015.12.005.

Draper, H.H., Hadley, M., 1990. Malondialdehyde determination as index of lipid peroxidation (https://doi:). Met. Enzym. 186, 421–431. https://doi.org/10.1016/0076-6879(90)86135-i.

Eldh, M., Ekström, K., Valadi, H., Sjöstrand, M., Olsson, B., Jernås, M., Lötvall, J., 2010. Exosomes communicate protective messages during oxidative stress; possible role of exosomal shuttle RNA. PLoS One 5, e15353. https://doi.org/10.1371/journal.pone.0015353.

Ferreri, C., Sansone, A., Buratta, S., Urbanelli, L., Costanzi, E., Emiliani, C., Chatgilialoglu, C., 2020. The n-10 fatty acids family in the lipidome of human prostatic adenocarcinoma cell membranes and extracellular vesicles. Cancers 12, 900. https://doi.org/10.3390/cancers12040900.

Ferreri, C., Sansone, A., Krokidis, M.G., Masi, A., Pascucci, B., D'Errico, M., Chatgilialoglu, C., 2022. Effects of oxygen tension for membrane lipidome remodeling of cockayne syndrome cell models (https://doi:). Cells 11, 1286. https://doi.org/10.3390/cells11081286.

Ferreri, C., Masi, A., Sansone, A., Giacometti, G., Larocca, A.V., Menounoum, G., Scanferlato, R., Tortorella, S., Rota, D., Conti, M., Deplano, S., Louka, M., Maranini, A.R., Salati, A., Sunda, V., Chatgilialoglu, C., 2016. Fatty acids in membranes as homeostatic, metabolic and nutritional biomarkers: recent advancements in analytics and diagnostics (https://doi:). Diagnostics 7, 1. https://doi.org/10.3390/diagnostics7010001.

Folch, J., Less, M., Sloane Stanley, G.H., 1957. A simple method for the isolation and purification of total lipids from animal tissues. J. Biol. Chem. 226, 497–509. https://doi.org/10.1016/S0021-9258(18)64849-5.

Fujita, Y., Araya, J., Ito, S., Kobayashi, K., Kosaka, N., Yoshioka, Y., Kadota, T., Hara, H., Kuwano, K., Ochiya, T., 2015. Suppression of autophagy by extracellular vesicles promotes myofibroblast differentiation in COPD pathogenesis. J. Extracell. Ves. 4, 28388. https://doi.org/10.3402/jev.v4.28388.

Garbin, U., Pasini, F., Stranieri, A., Cominacini, C., Pasini, M., Manfro, A., Lugoboni, S., Mozzini, F., Guidi, C., Faccini, G.C., Cominacini, L, G., 2009. Cigarette smoking blocks the protective expression of Nrf2/ARE pathway in peripheral mononuclear cells of young heavy smokers favouring inflammation. PLoS One 4, e8225. https://doi.org/10.1371/journal.pone.0008225.

Ghezzi, S., Risé, P., Ceruti, S., Galli, C., 2007. Effects of cigarette smoke on cell viability, linoleic acid metabolism and cholesterol synthesis, in THP-1 cells (https://doi:). Lipids 42, 629–636. https://doi.org/10.1007/s11745-007-3070-4.

Goldman, A., Harper, S., Speicher, D.W., 2016. Detection of Proteins on Blot Membranes. Curr. Protoc. Protein Sci. 86, 10.8.1–10.8.11. https://doi.org/10.1002/cpps.15.

Gordon, C., Gudi, K., Krause, A., Sackrowitz, R., Harvey, B.G., Strulovici-Barel, Y., Mezey, J.G., Crystal, R.G., 2011. Circulating endothelial microparticles as a measure of early lung destruction in cigarette smokers. Am. J. Respir. Crit. Care Med. 184, 224–232. https://doi.org/10.1164/rccm.201012-2061OC.

Gornati, R., Colombo, G., Clerici, M., Rossi, F., Gagliano, N., Riva, C., Colombo, R., Dalle-Donne, I., Bernardini, G., Milzani, A., 2013. Protein carbonylation in human endothelial cells exposed to cigarette smoke extract. Toxicol. Lett. 218, 118–128. https://doi.org/10.1016/j.toxlet.2013.01.023.

Haque, S., Kodidela, S., Sinha, N., Kumar, P., Cory, T.J., Kumar, S., 2020. Differential packaging of inflammatory cytokines/chemokines and oxidative stress modulators in U937 and U1 macrophages-derived extracellular vesicles upon exposure to tobacco constituents. PLoS One 15, e0233054. https://doi.org/10.1371/journal.pone.0233054.

Harischandra, D.S., Ghaisas, S., Rokad, D., Kanthasamy, A.G., 2017. Exosomes in toxicology: relevance to chemical exposure and pathogenesis of environmentally linked diseases. Toxicol. Sci. 158, 3–13. https://doi.org/10.1093/toxsci/kfx074.

Hirsova, P., Ibrahim, S.H., Krishnan, A., Verma, V.K., Bronk, S.F., Werneburg, N.W., Charlton, M.R., Shah, V.H., Malhi, H., Gores, G.J., 2016. Lipid-induced signaling causes release of inflammatory extracellular vesicles from hepatocytes (https://doi:). Gastroenterologist 150, 956–967. https://doi.org/10.1053/j.gastro.2015.12.037.

Hung, W.L., Hwang, L.S., Shahidi, F., Pan, M.H., Wang, Y., Ho, C.T., 2016. Endogenous formation of trans fatty acids: Health implications and potential dietary intervention. J. Funct. Foods 25, 24. https://doi.org/10.1016/j.jff.2016.05.006.

Kakazu, E., Mauer, A.S., Yin, M., Malhi, H., 2016. Hepatocytes release ceramide-enriched pro-inflammatory extracellular vesicles in an IRE1 -dependent manner. J. Lip. Res. https://doi.org/10.1194/jlr.M063412.

Kästle, M., Grune, T., 2011. Proteins bearing oxidation-induced carbonyl groups are not preferentially ubiquitinated. Biochimie 96, 1076–1079. https://doi.org/10.1016/j.biochi.2011.03.004.

Kästle, M., Reeg, S., Rogowska-Wrzesinska, A., Grune, T., 2012. Chaperones, but not oxidized proteins, are ubiquitinated after oxidative stress. Free Radic. Biol. Med. 53, 1468–1477. https://doi.org/10.1016/j.freeradbiomed.2012.05.039.

Kowal, J., Arras, G., Colombo, M., Jouve, M., Morath, J.P., Primdal-Bengtson, B., Dingli, F., Loew, D., Tkach, M., Théry, C., 2016. Proteomic comparison defines novel markers to characterize heterogeneous populations of extracellular vesicle subtypes. Proc. Natl. Acad. Sci. USA 113, E968–E977. https://doi.org/10.1073/pnas.1521230113.

Küçüksayan, E., Sansone, A., Chatgilialoglu, C., Ozben, T., Tekeli, D., Talibova, G., Ferreri, C., 2022. Sapienic acid metabolism influences membrane plasticity and protein signaling in breast cancer cell lines. Cells 11, 225 https://doi.org/10.3390/cells11020225 2022.

LeBel, C.P., Ischiropoulos, H., Bondy, S.C., 1992. Evaluation of the probe 2',7'-dichlorofluorescin as an indicator of reactive oxygen species formation and oxidative stress. Chem. Res. Toxicol. 5, 227–231. https://doi.org/10.1021/tx00026a012.

Lerner, N., Chen, I., Schreiber-Avissar, S., Beit-Yannai, E., 2020. Extracellular vesicles mediate anti-oxidative response-in vitro study in the ocular drainage system. Int. J. Mol. Sci. 21, 6105. https://doi.org/10.3390/ijms21176105.

Li, M., Yu, D., Williams, K.J., Liu, M.L., 2010. Tobacco smoke induces the generation of procoagulant microvesicles from human monocytes/macrophages. Arter. Throm. Vasc. Biol. 30, 1818–1824. https://doi.org/10.1161/ATVBAHA.110.209577.

Llorente, A., Skotland, T., Sylvänne, T., Kauhanen, D., Róg, T., Orłowski, A., Vattulainen, I., Ekroos, K., Sandvig, K., 2013. Molecular lipidomics of exosomes released by PC-3 prostate cancer cells. Biochim. Biophys. Acta 1831, 1302–1309. https://doi.org/10.1016/j.bbalip.2013.04.011.

Mobarrez, F., Antoniewicz, L., Bosson, J.A., Kuhl, J., Pisetsky, D.S., Lundbäck, M., 2014. The effects of smoking on levels of endothelial progenitor cells and microparticles in the blood of healthy volunteers. PLoS One 9, e90314. https://doi.org/10.1371/journal.pone.0090314.

Moon, H.G., Kim, S.H., Gao, J., Quan, T., Qin, Z., Osorio, J.C., Rosas, I.O., Wu, M., Tesfaigzi, Y., Jin, Y., 2014. CCN1 secretion and cleavage regulate the lung epithelial cell functions after cigarette smoke. Am. J. Physiol. Lung Cell. Mol. Physiol. 307, L326–L337. https://doi.org/10.1152/ajplung.00102.2014.

Reis, R., Orak, D., Yilmaz, D., Cimen, H., Sipahi, H., 2021. Modulation of cigarette smoke extract-induced human bronchial epithelial damage by eucalyptol and curcumin. Hum. Exp. Toxicol. 40, 1445–1462. https://doi.org/10.1177/0960327121997986.

Robbins, P.D., Akaitz, D., Booker, C.N., 2016. Regulation of chronic inflammatory and immune processes by extracellular vesicles. J. Clin. Investig. 126, 1173–1180. https://doi.org/10.1172/JCI81131.

Ryu, A.R., Kim, D.H., Kim, E., Lee, M.Y., 2018. The potential roles of extracellular vesicles in cigarette smoke-associated diseases. Oxid. Med. Cell. Longev. 2018, 4692081. https://doi.org/10.1155/2018/4692081.

Sagini, K., Costanzi, E., Emiliani, C., Buratta, S., Urbanelli, L., 2018b. Extracellular vesicles as conveyors of membrane-derived bioactive lipids in immune system. Int. J. Mol. Sci. 19, 1227. https://doi.org/10.3390/ijms19041227.

Sagini, K., Urbanelli, L., Costanzi, E., Mitro, N., C aruso, D., Emiliani, C., Buratta, S., 2018a. Oncogenic H-ras expression induces fatty acid profile changes in human fibroblasts and extracellular vesicles. Int. J. Mol. Sci. 19, 3515. https://doi.org/10.3390/ijms19113515.

Sansone, A., Melchiorre, M., Chatgilialoglu, C., Ferreri, C., 2013. Hexadecenoic fatty acid isomers: a chemical biology approach for human plasma biomarker development. Chem. Res. Toxicol. 26, 1703–1709. https://doi.org/10.1021/tx400287u.

Saxena, A., Walters, M.S., Shieh, J.H., Shen, L.B., Gomi, K., Downey, R.J., Crystal, R.G., Moore, M.A.S., 2021. Extracellular vesicles from human airway basal cells respond to cigarette smoke extract and affect vascular endothelial cells. Sci. Rep. 11, 6104. https://doi.org/10.1038/s41598-021-85534-6.

Scanferlato, R., Bortolotti, M., Sansone, A., Chatgilialoglu, C., Polito, L., De Spirito, M., Maulucci, G., Bolognesi, A., Ferreri, C., 2019. Hexadecenoic fatty acid positional isomers and De Novo PUFA synthesis in colon cancer cells. Int. J. Mol. Sci. 20, 832. https://doi.org/10.3390/ijms20040832.

Stassen, F.R.M., van Eijck, P.H., Savelkoul, P.H.M., Wouters, E.F.M., Rohde, G.G.U., Briedé, J.J., Reynaert, N.L., de Kok, T.M., Benedikter, B.J., 2019. Cell type- and exposure-specific modulation of CD63/CD81-positive and tissue factor-positive extracellular vesicle release in response to respiratory toxicants. Oxid. Med. Cell. Longev. 2019, 5204218. https://doi.org/10.1155/2019/5204218.

Tancini, B., Buratta, S., Sagini, K., Costanzi, E., Delo, F., Urbanelli, L., Emiliani, C., 2019. Insight into the role of extracellular vesicles in lysosomal storage disorders. Genes 10, 510. https://doi.org/10.3390/genes10070510.

Théry, C., Witwer, K.W., Aikawa, E., Alcaraz, M.J., Anderson, J.D., Andriantsitohaina, R., Antoniou, A., Arab, T., Archer, F., Atkin-Smith, G.K., Ayre, D.C., Bach, J.M., et al., 2018. Minimal information for studies of extracellular vesicles 2018 (MISEV2018): a position statement of the International Society for Extracellular Vesicles and update of the MISEV2014 guidelines. J. Extracell. Ves. 7, 1535750. https://doi.org/10.1080/20013078.2018.1535750.

Trajkovic, K., Hsu, C., Chiantia, S., Rajendran, L., Wenzel, D., Wieland, F., Schwille, P., Brügger, B., Simons, M., 2008. Ceramide triggers budding of exosome vesicles into multivesicular endosomes (https://doi:). Science 319, 1244–1247. https://doi.org/10.1126/science.1153124.

Urbanelli, L., Magini, A., Buratta, S., Brozzi, A., Sagini, K., Polchi, A., Tancini, B., Emiliani, C., 2013. Signaling pathways in exosomes biogenesis, secretion and fate. Genes 4, 152–170. https://doi.org/10.3390/genes4020152.

Van Der Toorn, M., Rezayat, D., Kauffman, H.F., Bakker, S.J., Gans, R.O., Koëter, G.H., Choi, A.M., van Oosterhout, A.J., Slebos, D.J., 2009. Lipid-soluble components in cigarette smoke induce mitochondrial production of reactive oxygen species in lung epithelial cells. Am. J. Physiol. Lung Cell. Mol. Physiol. 297, 109–115. https://doi.org/10.1152/ajplung.90461.2008.

Wang, X., Lin, H., Gu, Y., 2012. Multiple roles of dihomo-γ-linolenic acid against proliferation diseases (https://doi:). Lip. Health Dis. 11, 25. https://doi.org/10.1186/1476-511X-11-25.

Yarana, C., Carroll, D., Chen, J., Chaiswing, L., Zhao, Y., Noel, T., Alstott, M., Bae, Y., Dressler, E.V., Moscow, J.A., Butterfield, D.A., Zhu, H., St Clair, D.K., 2018. Extracellular vesicles released by cardiomyocytes in a doxorubicin-induced cardiac injury mouse model contain protein biomarkers of early cardiac injury (https://doi:). Clin. Cancer Res. 24, 1644–1653. https://doi.org/10.1158/1078-0432.CCR-17-2046.

Yokoi, A., Yoshioka, Y., Yamamoto, Y., Ishikawa, M., Ikeda, S.I., Kato, T., Kiyono, T., Takeshita, F., Kajiyama, H., Kikkawa, F., Ochiya, T., 2017. Malignant extracellular vesicles carrying MMP1 mRNA facilitate peritoneal dissemination in ovarian cancer. Nat. Commun. 8, 14470. https://doi.org/10.1038/ncomms14470.

Zhang, M., Tang, J., Shan, H., Zhang, Q., Yang, X., Zhang, J., Li, Y., 2018. p66Shc mediates mitochondrial dysfunction dependent on PKC activation in airway

epithelial cells induced by cigarette smoke. Oxid. Med. Cell. Longev. 2018, 5837123.
https://doi.org/10.1155/2018/5837123.